Journal of Biotechnology 379 (2024) 65–77

Contents lists available at ScienceDirect

Journal of Biotechnology

journal homepage: www.elsevier.com/locate/jbiotec

Comprehensive evaluation of recombinant lactate dehydrogenase production from inclusion bodies

Chika Linda Igwe [a,b], Jan Niklas Pauk [a,b], Don Fabian Müller [b], Mira Jaeger [b], Dominik Deuschitz [b], Thomas Hartmann [b], Oliver Spadiut [b,*]

[a] Competence Center CHASE GmbH, Hafenstraße 47-51, Linz 4020, Austria
[b] Institute of Chemical, Getreidemarkt 9, Vienna 1060, Austria

ARTICLE INFO

Keywords:
Recombinant production
Lactate dehydrogenase
Inclusion body
Refolding dynamics
Processing chain
Enzyme characterization

ABSTRACT

A broad application spectrum ranging from clinical diagnostics to biosensors in a variety of sectors, makes the enzyme Lactate dehydrogenase (LDH) highly interesting for recombinant protein production. Expression of recombinant LDH is currently mainly carried out in uncontrolled shake-flask cultivations leading to protein that is mostly produced in its soluble form, however in rather low yields. Inclusion body (IB) processes have gathered a lot of attention due to several benefits like increased space-time yields and high purity of the target product. Thus, to investigate the suitability of this processing strategy for *ldh*L1 production, a fed-batch fermentation steering the production of IBs rather than soluble product formation was developed. It was shown that the space-time-yield of the fermentation could be increased almost 3-fold by increasing q_s to 0.25 g g^{-1} h^{-1} which corresponds to 21% of $q_{s,max}$, and keeping the temperature at 37°C after induction. Solubilization and refolding unit operations were developed to regain full bioactivity of the *ldh*L1. The systematic approach in screening for solubilization and refolding conditions revealed buffer compositions and processing strategies that ultimately resulted in 50% product recovery in the refolding step, revealing major optimization potential in the downstream processing chain. The recovered *ldh*L1 showed an optimal activity at pH 5.5 and 30°C with a high catalytic activity and K_M values of 0.46 mM and 0.18 mM for pyruvate and NADH, respectively. These features, show that the here produced LDH is a valuable source for various commercial applications, especially considering low pH-environments.

1. Introduction

The enzyme Lactate dehydrogenase (LDH) is an ubiquitous enzyme in a variety of living organisms, including bacteria, plants and animals as it is part of the glycolytic pathway (Nadeem et al., 2014. It catalyzes the bidirectional conversion of lactate to pyruvate by the use of NAD^+ (Burgner and Ray, 1984. As diverse as its hosts, so are the characteristics of the enzyme depending on its origin. With varying molecular masses and quaternary structures, their pH-stabilities range from more acidic to slightly basic environments with temperature optima between ambient and thermophilic temperatures. Thus, a variety of studies has been published investigating the characteristics of different LDHs (Table 1). Subsequently, besides the use of LDH as biomarker for the indication of various diseases, especially cancer (Puranik et al., 2021; Di Stefano et al., 2016, the potential of isolated LDH for commercial applications has been realized. These include the synthesis of D-phenyllactic acid (PLA) for the application as food preservatives (Luo et al., 2020; Jia et al., 2010 or production of various drug targets (Singh et al., 2012. Additionally, immobilized LDH is also used in the production of biosensors for e.g. lactate detection (Garcia et al., 2016; Rathee et al., 2016. Here, application fields include the food industry (e.g. wine and dairy industry (Istrate et al., 2021), clinical diagnostics (Kucherenko et al., 2019, or nutrition and health-care (Rayappan et al., 2019. In the field of sports performance in particular, bodily fluids (e.g. blood or sweat) are used to monitor lactate in real-time (Garcia et al., 2016. For the use as biosensors, LDH is often isolated from rabbit or pig muscle (Kumar et al., 2023; Istrate et al., 2021; Tsai et al., 2007. Thus, to endorse more sustainable production pathways, recently the attention was drawn to recombinant LDH expression. Consequently, the characteristics of heterologous LDH has been studied for multiple LDHs originating from a variety of different origins (Table 1).

Escherichia coli is a relevant host organism when it comes to

* Corresponding author.
E-mail address: oliver.spadiut@tuwien.ac.at (O. Spadiut).

https://doi.org/10.1016/j.jbiotec.2023.11.006
Received 29 September 2023; Received in revised form 22 November 2023; Accepted 23 November 2023
Available online 29 November 2023

Table 1
Comparison of recombinant LDH production processes with *E. coli* and enzyme characteristics.

LDH	Origin	MW [kDa]	Expression & Purification	pH_{opt} [-]	T_{opt} [°C]	K_M [mM]	k_{cat} [s^{-1}]	Application	Source
lrldh	*Lactobacillus rossiae*	39	soluble, IMAC	6.5	40	2.83[†]	12.29[†]	PLA production	Luo et al. (2020)
ldhL1	*Lactobacillus plantarum SK002*	35	soluble, IMAC	6	30	3.96[†]	ND	PLA production	Jia et al. (2010)
ldLDH	*Lactobacillus delbrueckii*	30	soluble, IMAC	7–7.5	55	1.34*	1.603*	detection of ALT	Sun et al. (2021)
TaLDH	*Theileria annulata*	ND	soluble, IMAC	ND	ND	0.1324*	44.5*	ND	Nural et al. (2016)
D-LDH	human	ND	soluble, IMAC	7	ND	ND	ND	ND	Torkzadeh-Mahani et al. (2020)
ND	*Lactobacillus sp. ZX1*	45	soluble, IMAC	6	ND	2.356[†]	10.71[†]	PLA production	Zhou et al. (2018)
ND	*Leuconostoc mesenteroides*	ND	soluble, IMAC	8	30	0.043*/0.089[+]	320*/757[+]	PLA production	Zaboli et al. (2021)
LDH-GT	*Geobacillus thermodenitrificans*	34.8	soluble, SEC	7.5	65	0.045*	ND	ND	Nadeem et al. (2018)
L-nLDH	*Bacillus coagulan*	34–36	soluble, IMAC	6.5	55	ND	ND	ND	Jiang et al. (2014)
ldh-1	*Litopenaeus vannamei*	ND	IBs, Chitin affinity chromatography & refolding	7.5	44	ND	ND	ND	Leyva-Carrillo et al. (2019)
PfLDH	*Plasmodium falciparum*	ND	soluble, IMAC	ND	ND	0.054*/0.0143	2.2×10^4	anti-malarial drug target	Berwal et al. (2008)
LF-D-LDH0653	*Lactobacillus fermentum*	43	ND	8	50	ND	ND	ND	Chen et al. (2017)
Dye-DLDH	*Candidatus Caldiarchaeum*	51	soluble, IMAC	9	50	ND	ND	lactate biosensor	Satomura et al. (2018)
LDHvan-2	*Litopenaeus vannamei*	140	soluble, Chitin affinity chromatography	7.5	50	0.203*/0.023[+]	78×10^3	ND	Fregoso-Peñuñuri et al. (2017)
rLDH	rat	117	soluble, IEX, SEC	ND	ND	0.53*	ND	ND	Nowicki et al. (2015)
LDH	*Lactobacillus plantarum*	ND	soluble & IBs, IMAC & refolding	ND	ND	ND	ND	ND	Togashi et al. (2009)
LDH-B	*Bubalus bubalis*	35	soluble & IBs, IEX & refolding	8	35	0.05	ND	ND	Nadeem et al. (2014)

ND: not defined, IMAC: Immobilized-metal-affinity chromatography, ALT: alanine aminotransferase, MW: molecular weight, PLA: D-phenyllactic acid, Substrates used for enzymatic characterization: * pyruvate, [+] NADH, [†] phenylpyruvic acid (PPA).

heterologous expression of proteins and robust bioprocessing (Kopp et al., 2019. However, as a stress response, often occurring upon overexpression of recombinant protein production, *E. coli* tends to form insoluble granules of the target product, so called inclusion bodies (IBs) (Bhatwa et al., 2021. Despite being mostly inactive protein aggregates, IBs pose a valuable source of pure and concentrated product (Singhvi et al., 2020; Slouka et al., 2019. Although the isolation step is mainly straightforward, an extensive downstream processing chain is required to recover the bioactive protein (Fig. 1) (Pauk et al., 2021; Buscajoni et al., 2022; Siew and Zhang, 2021. Therefore, upstream processes (USPs) with *E. coli* are often designed to express target proteins in soluble form using fusion-tags for simplified purification of the product (Bhatwa et al., 2021; Zhu et al., 2013. However, in contrast to the intended goal of this processing strategy Zhu et al. (2013) showed that the use of affinity tags often even triggers the formation of IBs. Also adaptation of cultivation conditions favoring expression of soluble protein does not always prevent IB formation entirely. In addition, the identification of classical process parameters like higher feeding rates, temperature shifts or certain pH-environments as key parameters in efficient IB processing guided the way to robust USPs with high space-time-yields (STYs) and product titers. Thus, compared to the soluble expression of proteins, the processing time of the USP can be reduced making the overall process more efficient (Nadeem et al., 2014; Margreiter et al., 2008; Slouka et al., 2018; Kopp et al., 2018.

For IB processes, following the USP and cell disruption step, misfolded protein structures isolated as IBs must be renatured into their native conformation (Fig. 1). Therefore, in a first step, the protein structure is completely denatured by harsh conditions using chaotrophic agents (e.g. urea and guanidine hydrochloride (GuHCl)), or mild solubilization conditions (e.g. pH-shifts or detergents) targeted at preserving as much of the secondary structure as possible (Singh et al., 2015. Afterwards, folding is enhanced by providing a favorable environment, often initiated by rapid reduction of the denaturing substance (Humer and Spadiut, 2018. It is well characterized that upon initialization, there is a competition between protein refolding, which is known to be of first order, and protein aggregation, which is assumed to be of higher order (Clark, 2004; Buscajoni et al., 2022. Thus, state-of-the-art processing mode is a batch dilution approach where the solubilized protein is diluted into huge amounts of buffer with the goal of reducing aggregation for increased yields (Pauk et al., 2021. The addition of chemical additives, separated into aggregation inhibitors or protein stabilizers, can further increase efficiency of protein refolding processes thereby boosting recovery yields (Buscajoni et al., 2022; Yamaguchi and Miyazaki, 2014.

Still, recombinant LDH is predominantly expressed in its soluble form in *E. coli* before being purified via the use of purification tags and affinity chromatography (Table 1). However, Nadeem et al. (2014) found that the cloning and expression of LDH from River Buffalo apart from soluble LDH also resulted in a IB fraction of the target product. Using a pulsed-refolding approach in combination with simple ion-exchange chromatography, they were able to obtain bioactive protein from the IB fraction in addition to the active protein that was expressed in its soluble form. Subsequently they made the entire LDH production process more economically feasible by utilizing both fractions with high recovery yields (Nadeem et al., 2014. Furthermore, the recombinant production of LDH led to soluble production as well as to IB formation in the study conducted by Togashi et al. (2009). There, solubilization and subsequent refolding of the IB fraction with zeolite beta led to a final refolding recovery yield of 40%.

Recombinant LDH is an interesting product for a variety of commercial applications, and compared to LDH isolated from animals, especially advantageous regarding sustainability and ethical concerns. However, to hold up against state-of-the art production from animals in terms of costs and effort, the recombinant production chain including fermentation and all downstream processing (DSP) unit operations need to be optimized. Recombinant production of LDH is mostly done in

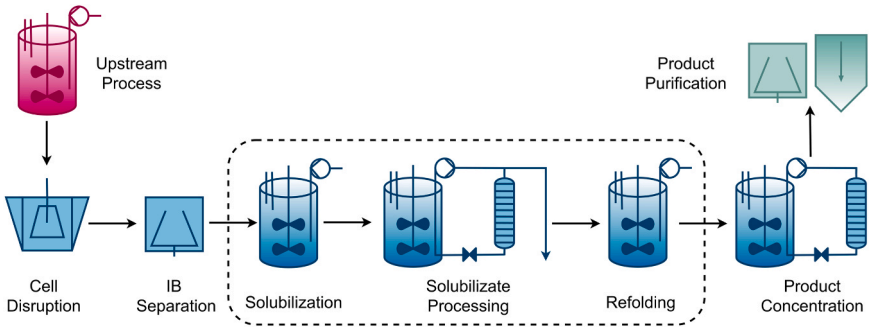

Fig. 1. Processing chain of inclusion body production with *E. coli*. Following controlled bioreatcor cultivations (red), bioactive product is obtained (blue) by (i) disrupting the harvested biomass, (ii) separating the IBs from cell debris by washing and centrifugation, (iii) solubilization and processing of the solubilized protein, (iv) refolding, (v) and concentration of the refolded protein. Finally, if necessary, the target product is further purified and polished (green). The highlighted section represents the critical unit operations during recovery.

Table 2
Induction conditions of two *E. colildh*L1 fed-batch processes.

Process	Induction Temperature in°C	q_s in g g^{-1} h^{-1}	Time of Harvest in h
I	30°C	0.15	12
II	37°C	0.25	6

shake-flasks and information on controlled bioprocesses with quantification of productivity and recovery yields are scarce. As IBs pose a valuable source of concentrated product, this publication aims at investigating if targeted IB production of recombinant LDH derived from *Lactobacillus plantarum* (*ldh*L1) is an alternative to common soluble processing strategies. Thus, fermentations were carried out in addition to the systematic development of a DSP chain. Different fermentation conditions were compared in a controlled bioreactor set-up, while the yield of soluble *ldh*L1 was compared to the IB fraction. In addition, for the product expressed in IBs, a DSP chain was developed and tailored for conditions enabling elevated product recovery. However, currently the STY of the entire production chain of IB processes is often inferior in comparison to the soluble production of affinity-tagged proteins featuring fewer processing steps. Therefore, to enable the full optimization potential of IB processing, all unit operations were systematically investigated to find the major bottle-necks of this production platform. Additionally, enzyme characterization studies aim to show the potential of the here expressed *ldh*L1 for acidic pH-applications.

2. Material and methods

2.1. Strain and model enzyme

E. coli BL21 (DE3), pET28a(+) expression vector and a T7 promoter were used to express L-Lactate dehydrogenase 1 originating from *Lactobacillus plantarum*. A His_6-tag for product concentration via affinity chromatography was fused to the C-terminus.

2.2. Cultivation and protein expression

Pre-cultures of *E. coli* were grown in DeLisa defined medium (DeLisa et al., 1999 (50 μg mL^{-1} ampicillin, 8.8 g L^{-1} glucose) in baffled shake flasks in an Infors HR Multitronshaker (Infors AG, Bottmingen, Switzerland) for 16 h at 37°C. Main cultures were cultivated in a 3.3 L Labfors bioreactor (Infors AG, Bottmingen, Switzerland) at 37°C. The process was inoculated by dilution of the pre-culture (5%, v/v) into 2.0 L of DeLisa batch medium (DeLisa et al., 1999 (50 μg mL^{-1} ampicillin, 15 g L^{-1} glucose). After substrate depletion a fed-batch phase with an exponential feed profile was conducted using glucose at a concentration of 440 g L^{-1} and by setting a specific glucose uptake (q_s) of 0.25 g g^{-1} h^{-1}. A constant pH of 7.0 was assured by addition of 12.5% ammonium hydroxide (v/v) and 2 M phosphoric acid. The dissolved oxygen tension was controlled above 30% by variation of agitation (800–1200 rpm) and the oxygen mole fraction in the inlet gas flow (20.95–24.11% (v/v)). After induction of protein expression with 1 mM isopropyl-D-thiogalactopyranoside (IPTG), the q_s as well as the cultivation temperature were adapted (Table 2). Samples were taken automatically in regular intervals, cooled (4°C) and analyzed. Glucose concentrations were determined using an enzymatic analyzer (Cedex Bio HT, Roche, Basel, Switzerland), the optical density (OD) was measured at a wavelength of 600 nm, dry cell weight (DCW) was determined in triplicates after drying at 105°C for 24 hours.

Table 3
Conditions of full-factorial DoE for screening of solubilization conditions.

Parameter	GuHCl in M	Buffer strength in mM	pH –	IB concentration in g wet IB L^{-1}
Range	2–6	50–150	6–9	20–100

2.3. Experimental planning and analysis

A Design-of-experiment (DoE) approach was used for the development of solubilization and refolding conditions. Planning and analysis was conducted using the software MODDE® (Sartorius, Bottmingen, Switzerland). Data evaluation and model fitting was conducted using Python 3.7. For the development of the refolding conditions, a multi-objective optimization was conducted respecting the two distinct objectives (minimization of protein aggregation and maximization of protein refolding yield) dependent on two process parameters (protein and GuHCl concentration). In the first instance a polynomial model was computed to describe the dependency of both objective variables on the parameters. These model functions were then used as cost functions for the multi-objective optimization (MOO) with opposite signs. A genetic algorithm was used as an optimizer to solve the optimization problem. The resulting conditions were then used to adapt the dilution factor (DF) in the scaled batch refolding process.

2.4. Protein isolation, solubilization and refolding

Harvested biomass (BM) was centrifuged (16,000 xg, 25 min, 4°C) before the obtained biomass pellet was stored at − 20°C until further processing. The thawed biomass was then resuspended in lysis buffer (100 mM Tris-HCl, 10 mM ethylenediaminetetraacetic acid (EDTA), pH 7.4) at a concentration of 150 g wet BM L^{-1}. Cells were ruptured at high pressure (1200 bar, three cycles) using a PandaPlus 2000 Lab Homogenizer (GEA group, Düsseldorf, Germany). The supernatant was removed after centrifugation (13,000 xg, 20 min, 4°C). Separation of IBs and cell debris was achieved by centrifugation following a two-step

Table 4
Conditions of full-factorial DoE to analyze the influences of additives on aggregation and enzymatic activity.

Parameter	Dilution –	Glycerol in % (w/v)	Trehalose in M	Tween-80 in M	KCl in M
Range	10–40	0–20	0–0.5	0–0.0005	0–0.5

washing process (Buffer I: 50 mM Tris-HCl, 0.5 M NaCl, 0.02% Tween 80 (w/v), pH 8.0, Buffer II: 50 mM Tris-HCl, 5 mM EDTA, pH 8.0).

A solubilization DoE was conducted in full-factorial design. Parameters and ranges were based on comparable literature and are shown in detail in Table 3. The solubilization efficiency in % was used as response. Solubilization of the IBs was investigated in reaction tubes after thawing of the frozen IBs at room temperature (RT). Solubilization buffer was added to the reaction tube to obtain a defined concentration of g wet IB L^{-1}. The mixture was incubated for 2 h under slight agitation, centrifuged (20,000 xg, 10 min, 4°C), and the supernatant containing the solubilized protein was used for refolding processes.

Small-scale refolding was investigated in reaction tubes at a final volume of 1.5 mL. The reaction was started by rapid dilution adding the solubilized protein into the pre-cooled refolding buffer. The samples were incubated for 2 h at 4°C under slight agitation. The buffer was based on the results found in the solubilization DoE. The parameters with the highest impact were then also tested in the refolding step, namely pH (4.0–7.0) and buffer strength (100–200 mM). The impact of additives was tested with best conditions (150 mM sodium phosphate buffer, pH 6.0) using a full-factorial DoE approach, where the aggregation in g g^{-1} and the enzymatic activity in U mL^{-1} were used as response. Parameters and ranges were based on comparable literature and can be found in Table 4. Scaled batch refolding was carried out in a 3.3 L Labfors 5 stirred tank reactor (Infors AG, Bottmingen, Switzerland) at an initial volume of 0.8 L. The concentration of added solubilized protein and GuHCl was obtained by the results of the multi-objective-optimization. The solubilized protein was rapidly added into pre-cooled refolding buffer (150 mM phosphate buffer, pH 6.0), resulting in 0.5 g L^{-1} protein and 0.15 M GuHCl. The temperature was set to 10°C by connection of a Lauda Alpha R8 thermostat (Lauda, Königshofen, Germany) to the cooling system of the vessel. Agitation at 200 rpm was achieved by Rushton turbine impellers. A constant pH of 6.0 was controlled by addition of 0.2 M HCl and 0.5 M NaOH. Headspace aeration with pressurized air was kept at a flowrate of 1 vvm.

2.5. Protein purification and concentration

Immobilized-metal-affinity chromatography (IMAC) was performed on an ÄKTA Pure system (GE Healthcare, Chicago, IL, USA). Separation was conducted on a 5 mL HisTrap FF Crude column (Cytiva Europe GmbH, Freiburg, Germany). The column was equilibrated with binding buffer (20 mM sodium phosphate buffer, 500 mM sodium chloride (NaCl), 20 mM imidazole, pH 7.4). Gradient elution from 0% to 100% was carried out by increasing the imidazole concentration (20 mM sodium phosphate buffer, 500 mM NaCl, 500 mM imidazole, pH 7.4) within 4 column volumes (CV). The conductivity and absorbance at a wavelength of 280 nm was monitored. Collected fractions were analyzed regarding activity, purity and protein concentration. Removal of the imidazole was achieved by buffer exchange into a storage buffer (100 mM phospahte buffer, 50 mM trehalose, 100 mM L-arginin, pH 7.5) using PD MidiTrap G-25 all gravity columns (Cytiva Europe GmbH, Freiburg, Germany).

2.6. Analytical methods

2.6.1. Turbidity

Turbidity measurements were used to monitor aggregation. It was measured at a wavelength of 600 nm in a TECAN Spark® microplate reader (Tecan Trading AG, Männedorf, Switzerland). Measurements were conducted as technical triplicates.

2.6.2. Size exclusion chromatography

Size-exclusion-chromatography (SEC) was used to determine the concentration of native product. It was performed on a high-performance-liquid-chromatography (HPLC) Dionex UltiMate 3000 system (Thermo Fisher, Waltham, USA) with a BEH 200A SEC 1.7 μm, 4.6 × 300 mm, 3.5 μm column (Waters Corporation, Milford, USA) and an injection volume of 2 μL. Isocratic elution was carried out with potassium phosphate buffer (80 mM, pH 6.8, 250 mM KCl), for 18 minutes at a flow rate of 0.5 mL min^{-1}. The column oven was controlled at 25°C and absorbance was monitored at a wavelength of 214 nm and 280 nm.

2.6.3. Reversed-phase chromatography

Reversed-Phase-HPLC (RP) was used to determine the total concentration of *ldh*L1 and was carried out on a Polyphenyl BioResolve-RP-mAb 2.7 μm 3.0×100 mm column (Waters Corporation, Milford, USA), at a flow rate of 0.4 mL min^{-1}. The mobile phase contained Milli-Q® water supplemented with trifluoroacetic acid (TFA) (0.1%, v/v) on one line, and acetonitrile with TFA (0.1%, v/v) on another. The method was run for 10.4 min with gradient elution from 25% to 75% acetonitrile (v/v), and an injection volume of 8 μL. The column temperature was set to 70°C, absorbance was monitored at a wavelength of 214 nm and 280 nm (Kopp et al., 2020.

2.6.4. SDS-PAGE

Sodium dodecyl sulfate-polyacrylamide gel electrophoresis (SDS-PAGE) was conducted as described by Laemmli (1970). Samples were separated on a Mini-PROTEAN TGX Stain-Free Gels 4–15% gel at 180 V for 30 min and BioRad Precision Plus Protein Unstained Standards was used as molecular weight marker. Samples of solubilized protein were precipitated for removal of GuHCl by 10-fold dilution into pre-cooled acetone (− 20°C, 1 h) and consequent centrifugation (13,000 xg, 10 min, 4°C).

2.6.5. Total protein concentration

Total protein concentrations were determined using the Pierce™ BCA Protein Assay Kit (Thermo Fisher, Waltham, USA). A calibration curve consisting of bovine serum albumin standards (0.1 g L^{-1} to 1.0 g L^{-1}) was used for protein quantification.

2.7. Enzymatic characterization

2.7.1. Enzymatic activity assay

Enzymatic activity (EA) was determined via a photometric assay in a TECAN Spark® microplate reader (Tecan Trading AG, Männedorf, Switzerland). 133.4 μL of reaction buffer (100 mM sodium phosphate buffer, pH 5.5 or pH 7.5, 0.425 mM NADH, 0.45 mM pyruvate) were mixed with 66.6 μL of prediluted sample. Absorbance at a wavelength of 340 nm was measured for 3 minutes at a constant temperature of 30°C. The volumetric enzymatic activity was calculated based on equation (1), where the volumetric activity (vAc) in U mL^{-1} was calculated by the change in absorbance over time ($\Delta A/\Delta t$) in s^{-1}, the total assay volume (V_t) and the volume of the sample (V_s) in mL, the pathlength (l) in cm, the extinction coefficient of NADH (ϵ) in mM^{-1} cm^{-1} and the DF (Vanderlinde, 1985. Here one Unit of LDH activity was defined as the amount of enzyme that is necessary for the oxidation of one μmol of NADH per min.

$$vAc = \frac{V_t \cdot \frac{\Delta A}{\Delta t} \cdot DF}{V_s \cdot l \cdot \epsilon} \quad (1)$$

2.7.2. Determination of catalytical optima and stability

The pH-optimum for catalytic activity was determined using the following buffers at 100 mM: sodium citrate (pH 3.0–5.0), sodium

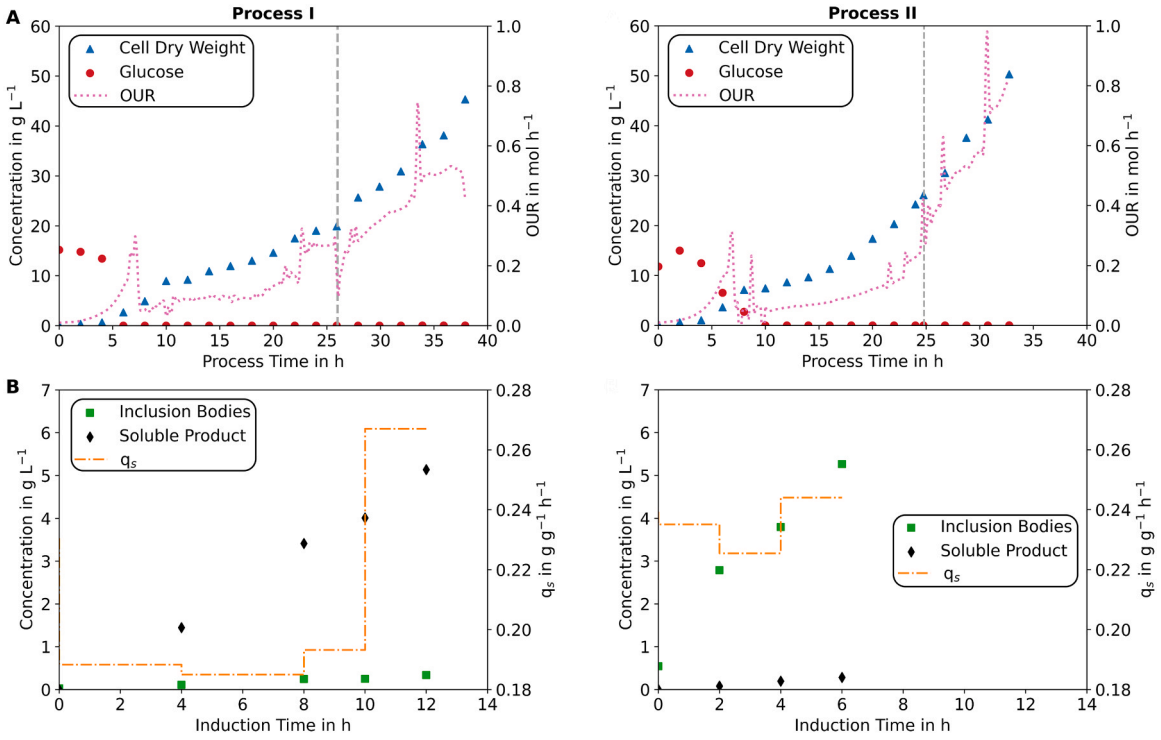

Fig. 2. Comparison of two *ldh*L1 production processes with varying induction conditions. (A) Cell dry weight and substrate concentration in g L^{-1} and oxygen uptake rate (OUR) in mol h^{-1} over processing time in h. Time of induction is indicated by grey line. (B) Product concentration in g L^{-1} and measured q_s in g g^{-1} h^{-1} over induction time in h. Separation of *ldh*L1 as IB and production of soluble product. Concentrations of glucose, soluble product and IBs are given as mean of technical duplicates.

phosphate (pH 5.5–8.0), Tris-hydrochloride (pH 9.0–10.0), carbonate bicarbonate (pH 11.0–12.0). At pH 7.5 the optimum temperature was determined by incubation of the assay solution for 5 minutes at different temperatures (25°C, 30°C, 35°C, 37°C, 42.5°C), before the assay was conducted at those temperatures. Temperature stability was determined at 30°C, 37°C and 45°C by incubation of the enzyme prior to determination of the enzymatic activity at 30°C. After sampling, samples were cooled to 4°C and centrifuged. The stability at different pH-values (5.5, 6.0, 7.0, 7.5) was conducted at 4°C. Samples were incubated at the respective pH at 4°C, before being centrifuged and analyzed. Kinetic constants were determined for two substrates, namely NADH (0.05–0.85 mM) and pyruvate (0.05–0.9 mM) by varying one concentration and keeping the other substance at a constant concentration. Characterization was conducted at two pH-values (5.5, 7.5) and a constant temperature of 30°C. A commercial LDH standard (CAS Nr. 9001–60–9) for comparison was purchased from ROTH (Karlsruhe, Germany) and diluted to the identical activity as the purified product. The enzyme kinetic parameters of the Henri-Michaelis-Menten equation (K_M, v_{max}) were identified from the observed data by non-linear least-square regression using Python 3.7.

3. Results and discussion

3.1. *ldhL1 production*

Recombinant LDH is often produced as soluble product in *E. coli* cultivations using an affinity tag for simplified purification. However, IB formation cannot always be entirely avoided as stress and stimulated overexpression can enhance accumulation of protein aggregates. Cultivation in bioreactors enables controlled and robust processing strategies and subsequently increased efficiency and higher yields. Thus, for protein production processes it was shown that the use of lower feed rates in combination with decreased temperatures after induction reduced IB formation facilitating the downstream process of tagged proteins of interest (Slouka et al., 2018; Nadeem et al., 2014.

Table 5
Key performance indicators of two *ldh*L1 production processes at the time of harvest.

Process	Biomass in g L^{-1}	Produced *ldh*L1 in g L^{-1}	Soluble Protein in $g_{P,sol}$ g_S^{-1}	IB yield in $g_{P,IB}$ g_S^{-1}	Productivity in $g_{P,tot}$ g_S^{-1} h^{-1}	STY in $g_{P,tot}$ h^{-1}
I	45.3	5.4	0.045	0.003	0.004	0.88
II	41.2	5.5	0.005	0.11	0.018	2.51

Comparing two *ldh*L1 fed-batch cultivation processes with different induction conditions (Table 2) showed that higher temperatures in combination with a high feed rate, indeed shifted the production of the expressed *ldh*L1 from soluble product to IB formation (Fig. 2). The key performance indicators (KPIs) listed in Table 5 allow comparison of the productivity of total produced *ldh*L1. It shows that the process targeted towards IB formation had a higher STY. Here, harvesting of the final fermentation broth took place six hours earlier in the case of IB enhancing conditions resulting in an almost 3-fold higher efficiency. Process II resulted in a final IB titer of 5.3 g L^{-1}, which is comparable to other studies on IB quality attributes highlighting the dependency of IB formation on feeding profile for two different proteins (Slouka et al., 2018. At low feed rates and reduced temperature (process I) only 4% of the final product was produced as IB while the remaining 96% of *ldh*L1 was expressed as soluble protein.

Although the STY could be increased by steering the process towards IB formation, soluble expression of tagged proteins has the major advantage of neglecting the requirement of multiple DSP steps, like it is necessary for IBs. On the other hand, in high-density cultivations a temperature downshift can become challenging at commercial scale. Here, an unstable temperature control as well as an increase in temperature might result in additional IB formation (Pekarsky et al., 2019;

Table 6
Buffer screening for *ldh*L1 IB solubilization conditions analyzed via a full-factorial DoE approach.

Response		Solubilization Efficiency* in %	
Factor	Range	Coefficient	p-value
IB Concentration	20–100 g L^{-1}	− 1,39	2.6×10^{-6}
GuHCl Concentration	2–6 M	2.69	0.005
Buffer Concentration	50–150 mM	1.76	1.7×10^{-5}
pH	6.0–9.0	− 1.50	0.004

*Model Parameters: $R^2 = 0.80$, $Q^2 = 0.96$.

Slouka et al., 2018.

In accordance with literature it was shown that during *ldh*L1 production, altering the fermentation conditions changed the way the majority of the product was expressed. Induction conditions that triggered IB formation were promising concerning the final productivity and STY of the USP. However, as both strategies of protein expression have their advantages and drawbacks, to make use of the benefits from IB an efficient DSP chain must be developed to obtain the bioactive protein.

3.2. Product recovery

3.2.1. Solubilization & refolding

The production of IBs comes with the major challenge of renaturing the bioactivity of the protein in a multi-step DSP chain. Thus, solubilization and refolding protocols need to be developed ensuring high product recovery yields to make use of the advantage of IB production processes. Therefore, with the goal of solubilizing the misfolded protein structures, variations of the concentration of the denaturing agent as well as of IBs in solution were investigated in combination with different buffer concentrations and pH-values. The results of the full-factorial DoE approach are listed in Table 6. Higher GuHCl concentrations in combination with lower IB concentrations led to elevated solubilization efficiency as it can be assumed that the IB pellet was more accessible for the buffer components. However, higher IB concentrations led to higher amounts of solubilized *ldh*L1 considering absolute protein concentrations. A low pH of 6.0 and a buffer concentration between 120–150 mM

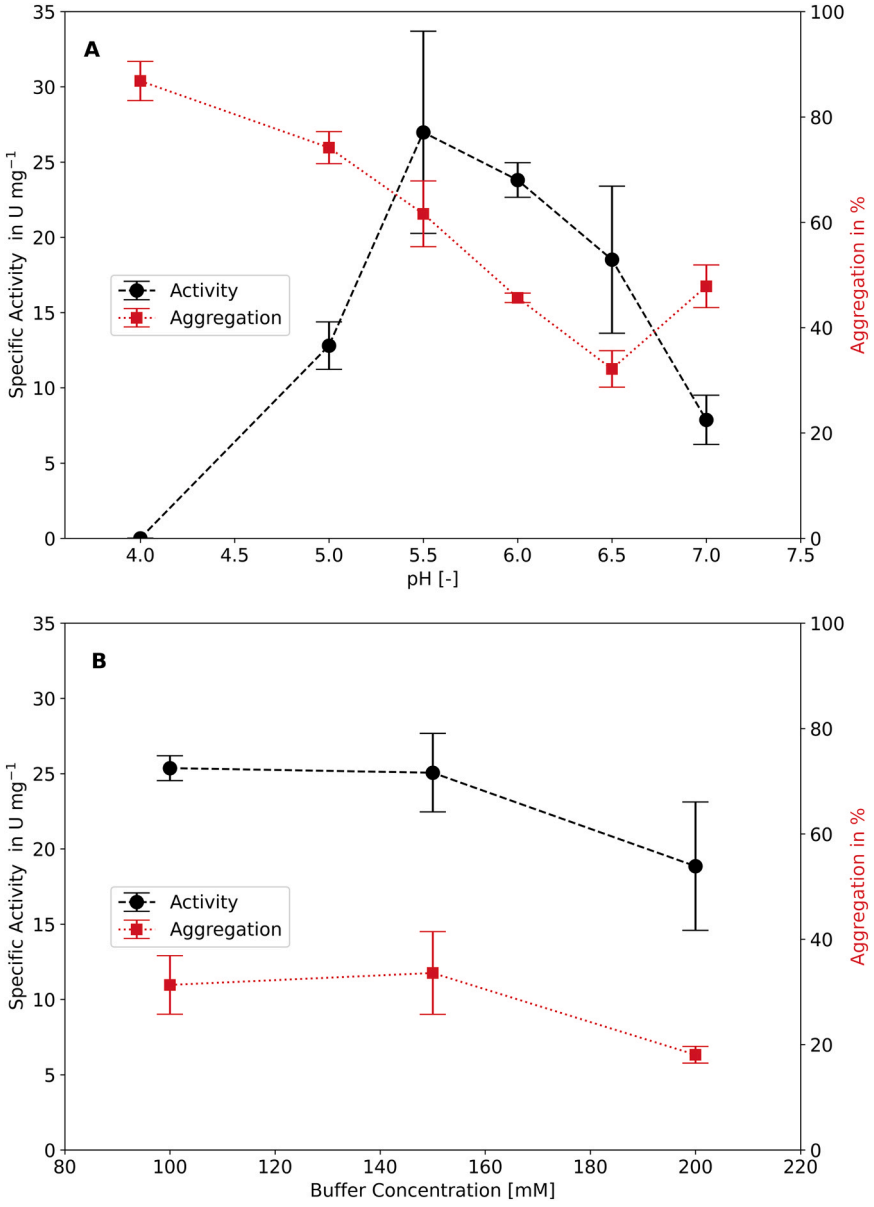

Fig. 3. The effect of different (A) pH-values and (B) buffer strength on refolding efficiency and aggregation yield in *ldh*L1 batch refolding processes. Composition of refolding buffer was adjusted using the final solubilization buffer without GuHCl as base. Rapid dilution was carried out at a DF of 40.

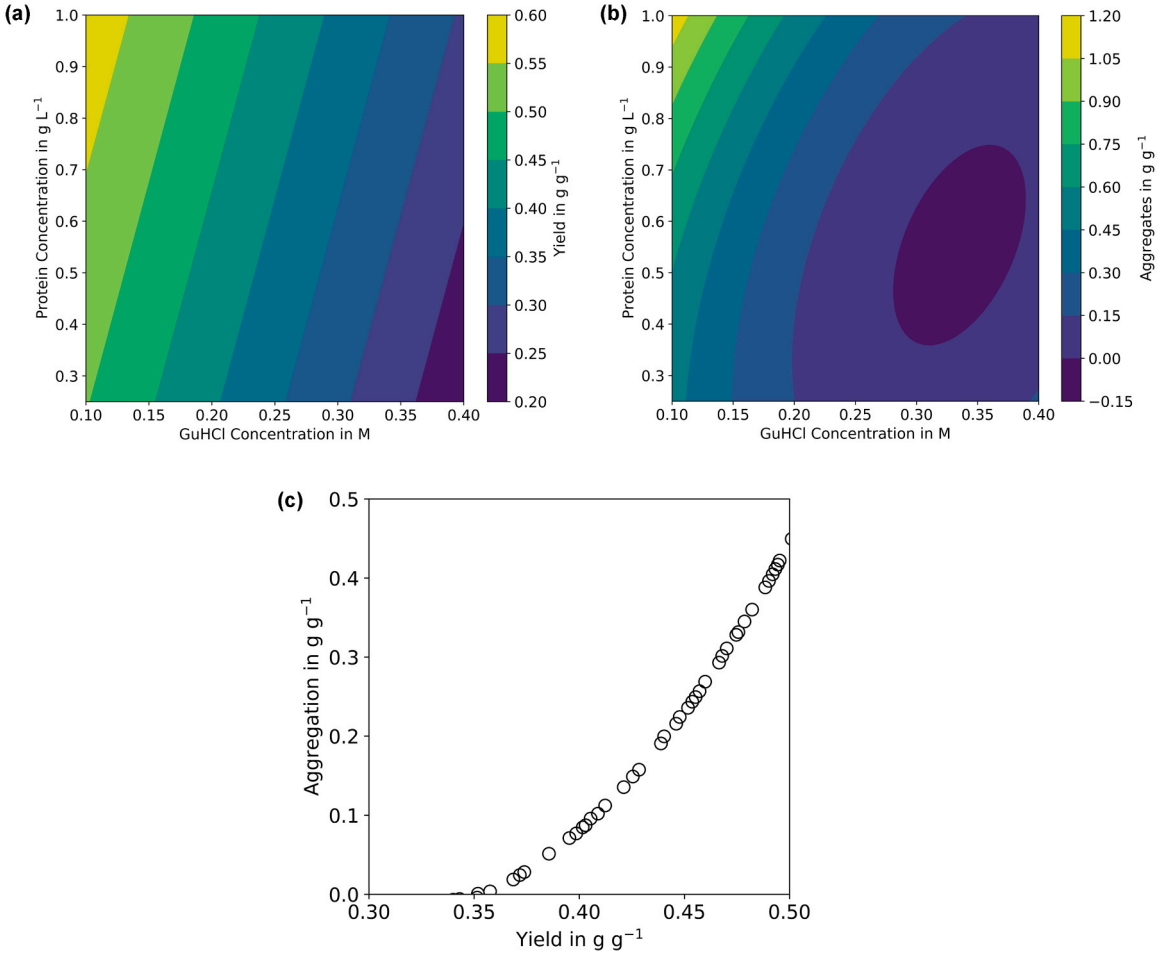

Fig. 4. Influence of GuHCl and protein concentration on refolding and aggregation yield. (A) Effect on the refolding yield is described by the function: $f(GuHCl, P) = 0.5727 - 0.966 \cdot GuHCl + 0.1067 \cdot P$. (B) Effect on the aggregate formation is described by the quadratic function: $f(GuHCl, P) = 1.035 - 6.335 \cdot GuHCl - 0.003602 \cdot P + 11.97 \cdot GuHCl^2 - 3.055 \cdot GuHCl \cdot P + 0.9283 \cdot P^2$. (C) Pareto diagram of optimal conditions defined by multi-objective-optimization.

positively influenced the solubilization yield. Efficient solubilization is often achieved at high pH-values (Humer et al., 2020; Singh et al., 2015. However, other studies revealed optimal pH-values that are in the neutral range as they highlight the correlation to the theoretical iso-electric point of the protein (Leyva-Carrillo et al., 2019. The higher buffer capacity that was shown to be beneficial for solubilization efficiency can impact the overall ionic strength of the buffer. Thus, using zeolite beta for refolding, during the denaturation step of the IB, Togashi et al. (2009) added sodium chloride to their solubilization buffer for increased recovery. In this case, the final solubilization buffer (150 mM sodium phosphate buffer, 4 M GuHCl, pH 6.0) at a concentration of 100 g wet IB L^{-1} led to a concentration of 10.18 ± 0.26 g L^{-1} solubilized *ldh*L1. For the development of the solubilization step, incubation times were not varied as it was observed that longer solubilization times (> 2 h) did not result in increased solubilization efficiency. However, for the best conditions, a solubilization time of 0.5 h resulted in less than 50% of the solubilized protein (data not shown), which is why the incubation time was not reduced below 2 h.

The most influential factors for solubilization of *ldh*L1 IBs were identified. As the interaction of the solubilization step with the refolding step is well known (Humer and Spadiut, 2018; Singh et al., 2015; Ebner et al., 2021, for *ldh*L1 refolding conditions were not developed from scratch, but based on the findings of the solubilization DoE. Therefore, the three most influencial factors were analyzed separately regarding their influence on the bioactivity of the *ldh*L1 and their effect on aggregation, namely buffer concentration (ionic strength), pH-value and concentration of GuHCl.

The importance of the pH-value for effective refolding of *ldh*L1 is underlined by the data presented in Fig. 3. Similar to the results that were found for the solubilization step previously, pH-values between 5.5 and 6.5 positively influenced the refolding yield, while even lower pH-values of 4.0 and 5.0 inhibited refolding. Subsequently, for those low pH-values the specific activities were very low while the aggregation increased to 87% and 74%, respectively. At the same time, aggregation was the lowest for a pH-value of 6.5, at 32%. Comparing different ionic strengths of the phosphate buffer revealed that neither specific activity nor aggregate formation were largely affected by the changing buffer concentrations (Fig. 3B). Finding a compromise between specific activity, and thus refolded product to fraction of aggregated protein, the pH for refolding of the solubilized *ldh*L1 was set to 6.0, while a buffer strength of 150 mM was chosen for further processing.

For batch refolding processes it is very important to find favorable protein concentrations to maximize the refolding yield. However, the process parameter protein concentration cannot be analyzed separately of the denaturant concentrations, as there is a carry over from the solubilization step (Ebner et al., 2021. Additionally, in their function as denaturing agent, chaotrophic substances are known to prevent aggregation in refolding processes, and thus are sometimes used as additives (Yamaguchi and Miyazaki, 2014; Buscajoni et al., 2022. However, compared to the solubilization unit operation, during refolding concentrations are usually lower to prevent complete denaturation of the bioactive product. To assess the influence of GuHCl and protein concentration on refolding yield and aggregate formation, different combinations of both process parameters were tested in batch refolding

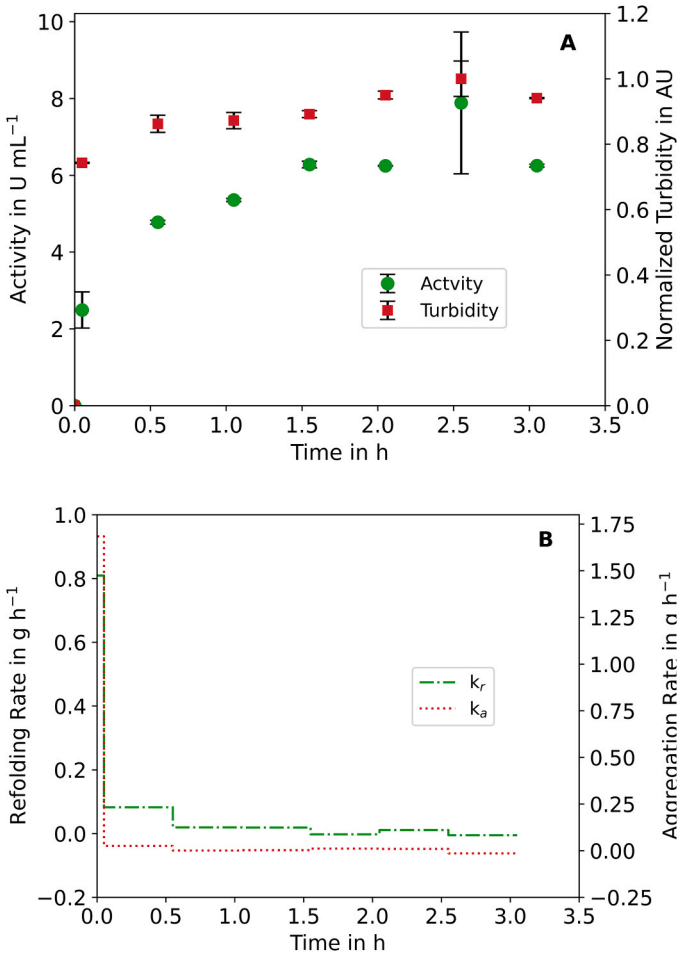

Fig. 5. Dynamics of a *ldh*L1 batch refolding process in bioreactor scale. (A) Volumetric activity in U mL^{-1} and turbidity in AU over process time in h. Samples were analyzed in technical replicates (n = 3). (B) Refolding and aggregation rates in g h^{-1} over process time in h.

processes. Models were fit to the data allowing extrapolation and estimation of ideal conditions.

Fig. 4 shows that increasing GuHCl concentrations decreased the formation of aggregates, while aggregation in general increased with higher protein concentrations. At the same time, the highest theoretical refolding yield can be achieved at low protein concentrations and low GuHCl concentrations. However, this is only valid in theory, as low concentrations of chaotropic agents always lead to aggregation, thereby lowering the final recovery yield. Thus, an MOO algorithm was used to identify not only the optimal conditions of GuHCl and protein concentration for increased yield and reduced aggregate formation, but also to incorporate realistic constraints. Thus Fig. 4C shows the most efficient solution by correlating a specific refolding and aggregation yield. Therefore values on the left side of the pareto-curve are less efficient for processing, while parameters on the right side of the curve are not achievable based on the gathered data. The pareto-diagram depicts that an increased yield always goes along with increased aggregation. However for lower yields, the aggregate formation is expected to be lower, leaving room for increasing processing efficiency by other parameters besides protein concentration and GuHCl. It can be assumed that most of the available protein did not undergo any reaction and thus is likely to be in an intermediate state that can still be influenced and directed towards refolding. In addition, the data show that with this processing strategy and buffer composition, the yield cannot be increased above 50%. Using the data obtained from the optimization problem, a scale-up process was conducted by adjusting dilution factor

Table 7
Influence of dilution and additives on aggregation and volumetric activity of *ldh*L1 refolding analyzed via full-factorial DoE approach.

Response		Aggregation* in g g^{-1}		Volumetric Activity‡ in U mL^{-1}	
Factor	Range	Coefficient	p-value	Coefficient	p-value
Dilution	10–40	− 7.58	5.0×10^{-7}	0.24	0.002
Glycerol	0–20% (w/v)	− 6.75	8.1×10^{-7}	0.166	0.02
Trehalose	0–0.5 M	0.83	0.003	ND	ND
Tween-80	0–0.0005 M	− 6.8	7.8×10^{-7}	ND	ND
KCl	0–0.5 M	0.8	0.003	ND	ND

ND: not defined (not significant). Model Parameters: $^{*}R^2 = 0.99$, $Q^2 = 0.99$, $^{‡}R^2 = 0.76$, $Q^2 = 0.47$.

and protein concentration in a way to maximize product recovery. The results of the process dynamics are presented in Fig. 5.

The presented data indicate that the majority of the refolding reaction was finalized after 2 h as the refolding rate approached 0.0 g h^{-1}. Most of the reaction happened instantaneously after initialization of the refolding process, where the refolding rate was at its maximum, before drastically decreasing 10-fold to 0.08 g h^{-1}. A similar dynamic progression was observed for the aggregation rate. However, here the rate indicated that no changes occurred after 0.5 h of processing. These dynamics, finally led to equal shares of the aggregation and refolding yield of 0.50 g g_{LDH}^{-1}, respectively. Although state-of-the art refolding in industry is commonly done in batch refolding approaches (Buscajoni et al., 2022, efficiency can be gained by alteration of the processing mode in addition to changes of the buffer composition itself. Strategies steering the process dynamics towards refolding rather than aggregate formation might be achieved by time-delayed addition of the solubilized protein to the refolding buffer. Here, common concepts include pulsed- or fed-batch dilution (Pauk et al., 2021; Buscajoni et al., 2022; Nadeem et al., 2014. As the refolding dynamics presented in Fig. 5 are mainly finalized after 2 h, a pulsed addition approach would present a possibility to further increase product recovery, while maintaining a similar STY. Recently, the use of process analytical technology in combination with model-based approaches has gathered major attention, thereby laying the basis for real-time monitoring and control strategies that would ultimately aid in increasing the yields of bioactive protein even further (Humer and Spadiut, 2018; Pauk et al., 2021.

Although a reduction of aggregation was shown to go along with increasing pH (Fig. 3), an aggregation rate of up to 50% reduces the efficiency of the entire processing chain as it results in a major loss of potential bioactive protein. Thus, different additives were tested for their effect on the final aggregated protein as well as on the resulting activity of the *ldh*L1 (Table 7).

The results show that increasing concentrations of glycerol and Tween-80 strongly reduced the formation of aggregates in batch refolding. Meanwhile the addition of trehalose and potassium chloride (KCl) resulted in even higher aggregate formation while these additives did not have an impact on the final *ldh*L1 activity. As it is known that the interaction of glycerol with the protein surface results in an elevated solvent ordering, thereby acting as stabilizing agent (Yamaguchi and Miyazaki, 2014, addition of glycerol did not only reduce aggregation but favorably influenced the *ldh*L1 refolding reaction (p-value <0.05). Similar to the results presented in this study, Ganjave et al. (2023) found that glycerol concentrations of up to 10% increased the refolding yield of fungal dehydrogenase IBs while higher glycerol concentrations were leading to increasing viscosity and subsequently to lower refolding yields. The negative influence of KCl on the refolding reaction also corresponds to the previously described findings, where changes of the ionic strength did not have significant effects on the refolding of *ldh*L1 IBs but showed decreasing tendencies with increasing ionic strengths (Fig. 3). The role of protein concentration in refolding reactions and its effect on aggregation has been excessively discussed (Clark, 2004; Pauk

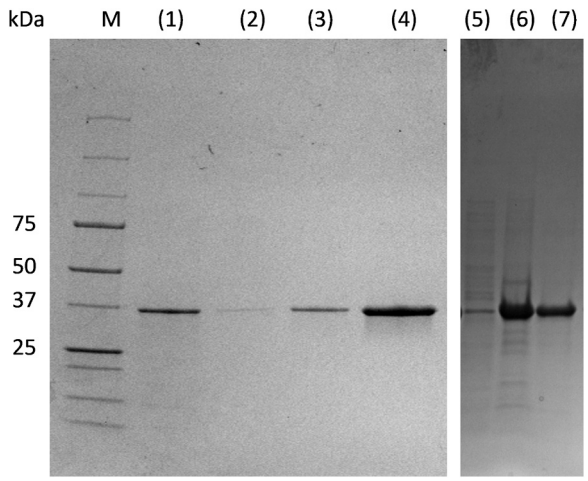

Fig. 6. SDS-PAGE analysis of isolated IBs, solubilized, refolded and purified *ldh*L1 from *L. plantarum*. (M) molecular weight marker, (1) refolded and centrifuged (load), (2) IMAC flow-through, (3) pooled fractions apart from main peak, and (4) main peak.(5) Supernatant after IB isolation, (6) isolated and washed IBs and (7) solubilized *ldh*L1 from a comparable process were compared regarding impurity patterns.

Table 8
Protein concentration, activities and purification factor of purification unit operation of refolded *ldh*L1.

	Volume in mL	Protein Concentration in g L^{-1}	Specific Activity in U mg^{-1}	Purification Factor
Refolding Load	120	0.64	26.54 ± 0.80	1
Active Side Peaks	9	0.50	25.26 ± 2.41	0.95
Active Main Peak	5	7.13	37.15 ± 0.26	1.40

et al., 2021. Thus, it comes as no surprise that the data depicted in Table 7 show that the highest impact on the responses comes from the dilution factor used for the refolding approach. Here, higher dilution factors and thus lower protein concentrations led to lower aggregate formation and vice versa. So with higher dilution factors and under beneficial buffer conditions a final yield of 0.5 g g^{-1} could be achieved in batch operation mode.

3.2.2. Purification

Fig. 6 shows purity patterns for the various processing steps, starting with isolated IBs until purified product after chromatography. The purified IBs still contained a lot of other proteins beside the *ldh*L1 (34.4 kDa). However, following the solubilization step the majority of these impurities was lost resulting in very light bands apart from the target band at 34.4 kDa. Thus, it can be assumed that only a low amount of impurities was carried over to the protein refolding step. To purify and concentrate the final product, the insoluble aggregates were removed from the harvested refolding mixture before capturing the *ldh*L1 via chromatography and storage of the product in appropriate buffer. Fig. 6 shows that the final product after IMAC and buffer exchange contained no other proteins besides the *ldh*L1 as shown by SDS-PAGE (line 3 and 4). In addition, SEC revealed a purity of > 99%. Comparing the purity to the load of the sample, which is the refolded product in solution separated from the aggregated fraction, reveals a similar purity of > 98% as shown by SEC and the absence of other proteins on the SDS-PAGE. It can be thus assumed that remaining impurities that were carried over from the solubilization step were removed with the insoluble aggregates after refolding. This is also represented by the data shown in Table 8. Here a purification factor of 1.4 indicates that the final protein was concentrated but was already quite pure prior to the chromatographic step. The recovery of the volumetric activity after the purification step was 69% while 54% of the protein concentration was recovered. Thus, concerning the here presented approach a further chromatographic purification might not be needed especially regarding the experimental effort and loss of product along the process.

3.3. Evaluation of inclusion body processing

The interest in IB processes has increased vastly. Thus, with the goal of investigating the suitability of this processing strategy for the production of *ldh*L1, the USP and DSP were investigated separately. It was shown that *ldh*L1 can be effectively produced in a controlled and scalable bioreactor set-up. Also, the strategy of producing IBs rather than soluble product were compared by quantitative tools. The systematic investigation across all unit operations regarding the production of *ldh*L1 as IBs revealed the KPIs of every unit operation separately. In addition, the product that was recovered throughout the entire processing chain could be followed (Fig. 7). The data show that regarding the final amount of IBs that are obtained via fed-batch fermentation,

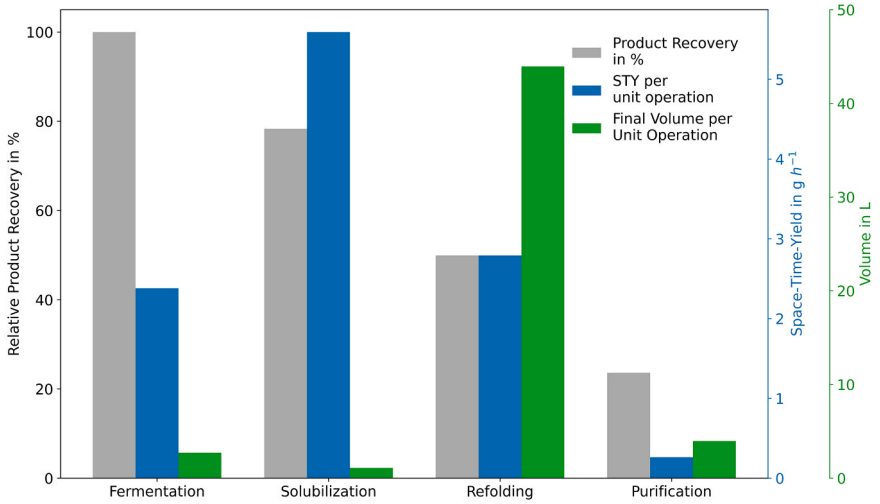

Fig. 7. Overview of KPIs per unit operation of *ldh*L1 IB production processes. The relative productivity is expressed as recovered *ldh*L1 in relation to the final fermentation yield. The *ldh*L1 STY in g h^{-1} and the maximum possible volume regarding the IB recovery in g refer to the various unit operations.

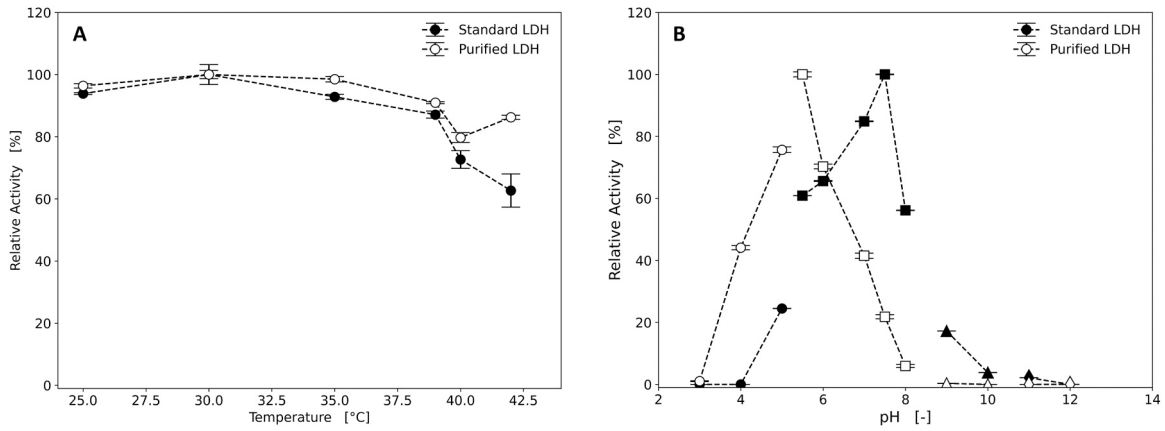

Fig. 8. Catalytic optima of purified and refolded *ldh*L1 in comparison to a commercial standard isolated from pig muscle. (A) For the determination of the temperature optimum samples and assay buffers were incubated for 5 min prior to analysis at the specified temperature. (B) The pH-optimum was analyzed by adjustment of the assay buffer to the various pH-values. Different marker styles connected by dashed lines indicate the different buffer systems used.

only 23% of the product can be recovered across the full processing chain. Here, the most inefficient unit operation was the refolding step, as the final titer and STY were low in comparison to the high volumes that would be necessary to process the entire harvested biomass of the USP. However, as discussed earlier, adaptation of the processing mode might most likely result in further increases of productivity. Thus, further investigation of the refolding unit operation is highly important to unlock the full potential of *ldh*L1 production. In addition, the resulting refolded product was shown to be already pure (98% purity) containing low amounts of impurities (Section 3.2.2) prior to the chromatographic step. Thus, to make the process more economically efficient, it might be beneficial to omit the chromatographic step and use a concentration step instead. The production of soluble protein with affinity tags always requires a chromatographic step as the purity is usually relatively low due to the presence of a variety of host-cell-proteins. Therefore, IB production can be advantageous if the IB and also the refolded product is already very pure. Meanwhile the STY of the solubilization step was already high which might also be related to the high purity of the solubilized protein (Fig. 6). During the solubilization step, the volume that is needed to solubilize an entire batch of IBs is low compared to the refolding step. Thus, within the here presented processing chain, the solubilization step is the unit operation with the highest recovery. Controlled USPs are known to have an effect on the downstream processing of IB processes (Slouka et al., 2018. Thus, purity could be further increased by steering the USP conditions as well as the conditions of cell disruption. Along the processing chain the major potential of improving this processing strategy is to increase the low product recoveries in the refolding unit operation. A change of the processing strategy as well as omitting the chromatographic step might increase final recovery yields. However, for tagged proteins soluble production still is a convenient choice as it reduces the effort in the subsequent DSP, especially as in this study the soluble protein was exhibiting similar KPIs as the purified product that was obtained from IBs. Here a specific activity of 24.23 ± 0.53 U mg^{-1} was reached at a purity of > 95% as determined by SEC after IMAC of the soluble product obtained by fermentation under mild conditions. Still regarding scaling capacity of the USP, IB processing might be a valid alternative if the product recovery can be optimized along the DSP chain.

3.4. Enzyme characterization

The purified *ldh*L1 was analyzed regarding its catalytic activity as well as its characteristics and compared to a commercial standard (ROTH, CAS Nr. 9001–60–9, Karlsruhe, Germany) which was derived from pig muscle.

Fig. 8A shows that the temperature optima of both enzymes were very similar. They both experienced their maximum relative activity at 30˚C, with no huge differences at 25˚C and 35˚C. Reduced activities for both enzymes were observed at higher temperatures, where the commercial standard was less active than the purified *ldh*L1. An optimal temperature of 30˚C is in accordance with reported literature values (Jia et al., 2010. The data presented in Fig. 8B show that the pH-optimum of the commercial standard is at a pH of 7.5 while the one of purified *ldh*L1 is two magnitudes lower at 5.5. These results are in accordance with literature, where LDHs derived from *Lactobacillus* species were shown to have their optimum activity at slightly acidic conditions (Table 1). However, the pH-optimum found within this study is slightly lower than reported for other LDHs from *L. plantarum* (Jia et al., 2010. The commercial standard still maintained 60% of its activity at 5.5, while the purified *ldh*L1 lost 78% of its activity at a pH of 7.5. Both enzymes were inactivated at a pH of 3.0 and pH-values above 9.0.

Table 9
Exponential decay of *ldh*L1 activities due to stability at different temperatures.

	Purified *ldh*L1		Commercial LDH		Fold change*	
Temperature	k_d in min^{-1}	$t_{1/2}$ in min	k_d in min^{-1}	$t_{1/2}$ in min	k_d	$t_{1/2}$
30°C	8.7×10^{-5}	7957	5.2×10^{-3}	133	192	60
37°C	1.3×10^{-4}	5333	5.1×10^{-3}	135	196	40
45°C	8.5×10^{-4}	812	5.9×10^{-2}	12	17	68

k_d: decay coefficient, $t_{1/2}$: half-time *fold increase ($t_{1/2}$) and fold decrease (k_d) of purified *ldh*L1 over standard LDH.

Analysis of the stability at different temperatures proofed the tendencies that were already observed during analysis of the temperature optima Fig. 8A. The enzymatic activity of both enzymes decreased severely at higher temperatures. At 30˚C the purified *ldh*L1 maintained almost 85% of its activity even after 2400 min. In comparison, the commercial standard lost above 90% of its activity during the same incubation period. The same progression was observed by increasing the temperature to 37°C. Here, the relative activities were a bit lower than at 30˚C. However, comparing the enzymatic decay at 45˚C it was found that both enzymes experienced a strong loss of activity. Here, the commercial standard lost more than 80% of its activity after only 10 min, leading to a half-time that is more than 10-fold lower than at 30°C (Table 9). In contrast, the half-time of the purified *ldh*L1 at 45˚C is still 80-fold higher than the half-time of the commercial standard at 30˚C.

The purified *ldh*L1 showed a similar loss of activity independent of

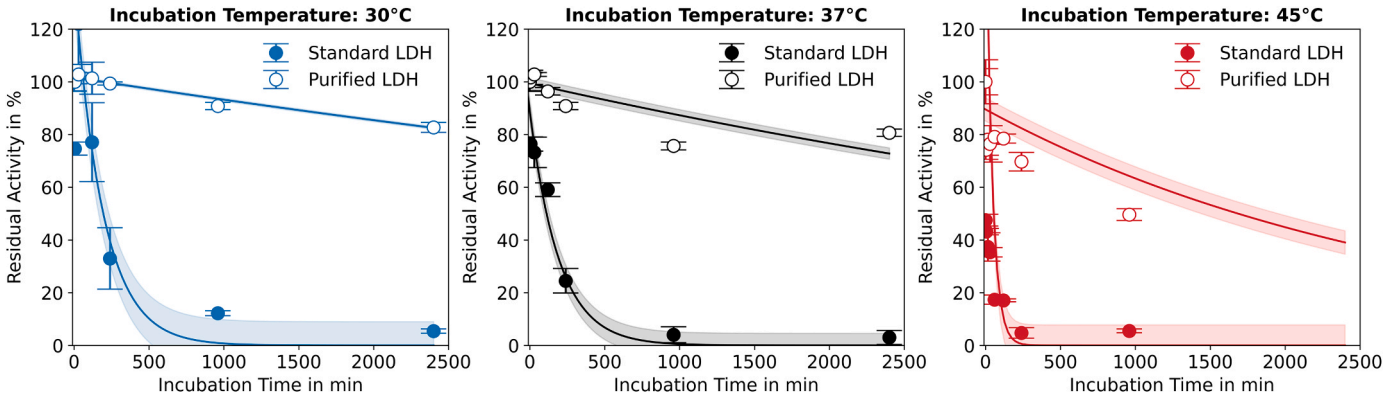

Fig. 9. Temperature stability of the purified *ldh*L1 in comparison to a commercial standard LDH isolated from pig muscle. Temperature stability was assessed at 30˚C, 37˚C and 45˚C. Samples were incubated at different temperatures and their activity was then measured at 30˚C. Exponential decay functions were fit to the data and were used to calculate kinetic parameters (k_D and $t_{1/2}$).

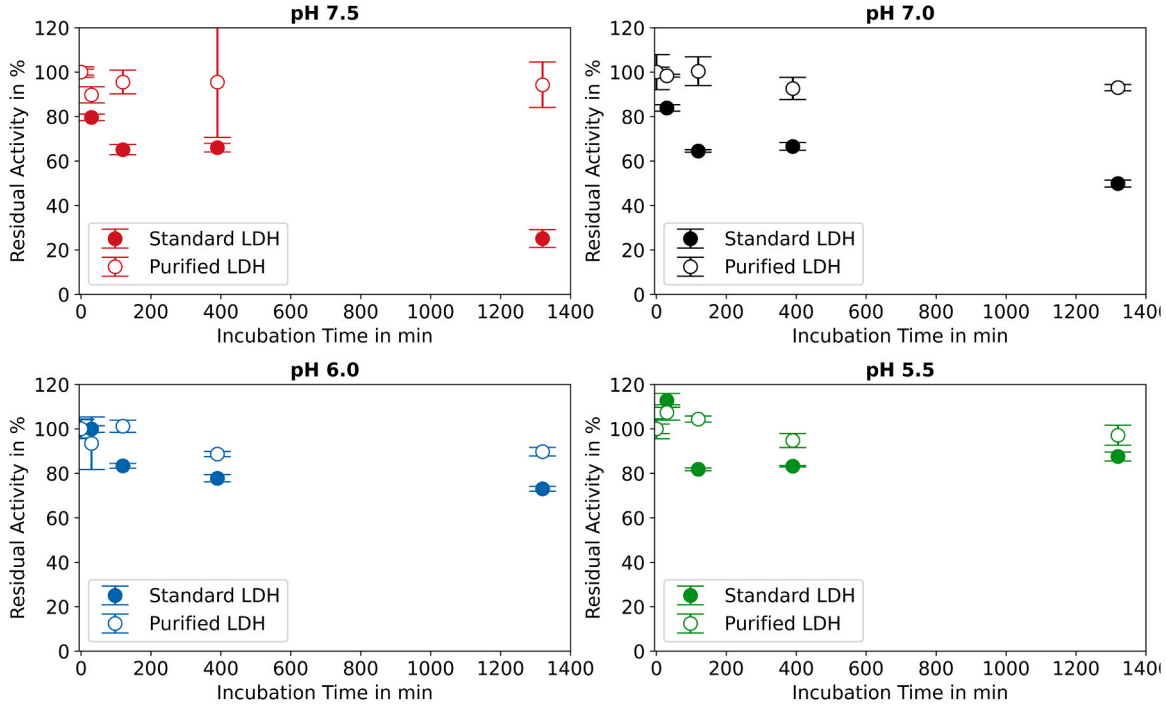

Fig. 10. pH-stability of the purified *ldh*L1 in comparison to a commercial standard LDH isolated from pig muscle. pH-stability was assessed at pH 5.5, pH 6.0, pH 7.0, pH 7.5. Samples were diluted into buffers at the corresponding pH-value. Incubation was conducted at 4˚C and and the activity was then measured at 30˚C.

Table 10
Kinetic properties of purified and refolded *ldh*L1 in comparison to a commercial standard isolated from pig muscle.

		Pyruvate			NADH		
		K_M in mM	k_{cat} in s^{-1}	k_{cat}/K_M in mM^{-1} s^{-1}	K_M in mM	k_{cat} in s^{-1}	k_{cat}/K_M in mM^{-1} s^{-1}
pH 5.5	Purified *ldh*L1	0.46 ± 0.02	56.04 ± 6.83	120.9	0.18 ± 0.03	106.99 ± 21.38	584.97
	Standard LDH	0.23 ± 0.04	51.31 ± 10.34	224.69	2.42 ± 0.36	0.16 ± 0.01	0.07
	Fold change*	2.0	1.0	0.5	0.07	668.7	8356.6
pH 7.5	Purified *ldh*L1	1.44 ± 0.56	4.67 ± 2.16	3.24	0.3 ± 0.11	9.17 ± 3.69	30.93
	Standard LDH	0.15 ± 0.03	53.77 ± 11.06	349.8	0.25 ± 0.07	26.72 ± 8.11	105.05
	Fold change*	9.6	11.5	108.0	1.2	0.4	3.4

*fold change of purified *ldh*L1 to standard LDH.

the pH-value (Fig. 10). The maximum loss of activity of 11% was at a pH of 6.0 after 390 min of incubation. The commercial standard exhibited similar behavior, however being more unstable at pH 7.0 and pH 7.5. As the pH-optimum for catalytic activity was at a pH of 7.5, it is interesting that the results presented in Fig. 9 showed a loss of activity of almost 40% after 390 min of incubation at the optimal temperature. The results indicate a superior stability of the here produced *ldh*L1 in comparison to commercially available standards that were expected to perform better

as they also find application in biosensors (Rathee et al., 2016).

The enzymatic characterization was done at both pH-optima of the respective LDH variants. The data in Table 10 depict a lower K_M value for the purified and refolded *ldh*L1 at the lower pH, while the commercial standard exhibited a lower K_M value at a pH of 7.5. The catalytic constant found for pyruvate were in the same order of magnitude as reported for other LDHs originating from similar species (Jia et al., 2010. A low turnover number for both substrates was reported for a pH-value of 7.5, which is in accordance to previous findings (Fig. 8). At their respective pH-optima, both enzymes seem to be similarly efficient towards the substrates pyruvate and NADH.

4. Conclusion

The *ldh*L1 originating from *L. plantarum* was shown to be specifically suitable for low pH-value applications which can be interesting for various applications like the biosensing of lactate in sweat. Having a catalytic optimum at a pH of 5.5 and a broad range of temperatures at which it is catalytically active, the here produced *ldh*L1 was shown to have a similar catalytic activity as commercially available standards, while its stability regarding pH-shifts and temperature increases proofed to be even superior. A processing chain, starting with a controlled *E. coli* fed-batch fermentation in a bioreactor, followed by solubilization and refolding unit operations in batch mode showed that IB processing is an alternative to soluble expression when it comes to *ldh*L1 production. The here presented strategy depicts a successful approach to produce *ldh*L1 at high titers with scalable methods. Still, investigation of the various DSP unit operations revealed some optimization potential to enable full potential of the USP. Here, a substantial increase of product recovery can be gained by further optimizing the processing mode of the refolding unit operation, by switching to a fed-batch strategy. The batch refolding yielded 50% of bioactive protein, leaving room for major process optimization. At the same time, high volumes are needed to refold an entire fermentation batch, resulting in excessive buffer consumption. Thus, either the buffer composition or the processing strategy could be further investigated. Alternatives could be pulsed addition of solubilized protein, fed-batch or continuous refolding. All in all, the here presented systematic investigation of all unit operations yields a robust processing strategy for the production of *ldh*L1. It was shown that advantages of IB production platforms like high purity and high STY in the fermentation are also valid for the production of recombinant LDH. Still, some knowledge based process development is needed to make the entire production process comparable to common production concepts.

CRediT authorship contribution statement

Spadiut Oliver: Writing – review & editing, Writing – original draft, Supervision, Project administration, Conceptualization. **Hartmann Thomas:** Investigation. **Deuschitz Dominik:** Investigation. **Igwe Chika Linda:** Writing – review & editing, Writing – original draft, Methodology, Investigation. **Jaeger Mira:** Investigation. **Müller Don Fabian:** Software, Formal analysis, Data curation. **Pauk Jan Niklas:** Methodology, Data curation.

Declaration of Competing Interest

The authors declared no competing interest.

Data Availability

Data will be made available on request.

Acknowledgments

The authors acknowledge financial support through the COMET Centre CHASE, funded within the COMET - Competence Centers for Excellent Technologies program by the BMK, the BMDW and the Federal Provinces of Upper Austria and Vienna. The COMET program is managed by the Austrian Research Promotion Agency (FFG). The authors also thank their project partner Bilfinger Life Science for the provided insights and support. Finally, the authors acknowledge TU Wien Bibliothek for financial support through its Open Access Funding Program.

References

Berwal, R., Gopalan, N., Chandel, K., Prasad, G.B.K.S., Prakash, S., 2008. Plasmodium falciparum: Enhanced soluble expression, purification and biochemical characterization of lactate dehydrogenase. Exp. Parasitol. 120, 135–141. https://doi.org/10.1016/j.exppara.2008.06.006.

Bhatwa, A., Wang, W., Hassan, Y.I., Abraham, N., Li, X.Z., Zhou, T., 2021. Challenges associated with the formation of recombinant protein inclusion bodies in escherichia coli and strategies to address them for industrial applications. Front. Bioeng. Biotechnol. 9.

Burgner, J.W.I., Ray, W.J.J., 1984. On the origin of the lactate dehydrogenase induced rate effect. Biochemistry 23, 3636–3648. https://doi.org/10.1021/bi00311a010 (publisher: American Chemical Society).

Buscajoni, L., Martinetz, M.C., Berkemeyer, M., Brocard, C., 2022. Refolding in the modern biopharmaceutical industry. Biotechnol. Adv. 61, 108050 https://doi.org/10.1016/j.biotechadv.2022.108050.

Chen, L., Bai, Y., Fan, T.P., Zheng, X., Cai, Y., 2017. Characterization of a d-Lactate dehydrogenase from lactobacillus fermentum JN248 with high phenylpyruvate reductive activity. J. Food Sci. 82, 2269–2275. https://doi.org/10.1111/1750-3841.13863.

Clark, P., 2004. Protein folding in the cell: reshaping the folding funnel. Trends Biochem. Sci. 29, 527–534. https://doi.org/10.1016/j.tibs.2004.08.008.

DeLisa, M.P., Li, J., Rao, G., Weigand, W.A., Bentley, W.E., 1999. Monitoring GFP-operon fusion protein expression during high cell density cultivation ofEscherichia coli using an on-line optical sensor. Biotechnol. Bioeng. 65, 54–64. https://doi.org/10.1002/(SICI)1097-0290(19991005)65:1<54::AID-BIT7>3.0.CO;2-R.

Di Stefano, G., Manerba, M., DiIanni, L., Fiume, L., 2016. Lactate dehydrogenase inhibition: exploring possible applications beyond cancer treatment. Future Med. Chem. 8, 713–725. https://doi.org/10.4155/fmc.16.10 (publisher: Future Science).

Ebner, J., Humer, D., Klausser, R., Rubus, V., Pell, R., Spadiut, O., Kopp, J., 2021. At-line reversed phase liquid chromatography for in-process monitoring of inclusion body solubilization. Bioengineering 8, 78. https://doi.org/10.3390/bioengineering8060078 number: 6 Publisher: Multidisciplinary Digital Publishing Institute.

Fregoso-Peñuñuri, A.A., Valenzuela-Soto, E.M., Figueroa-Soto, C.G., Peregrino–Uriarte, A.B., Ochoa-Valdez, M., Leyva-Carrillo, L., Yepiz-Plascencia, G., 2017. White shrimp Litopenaeus vannamei recombinant lactate dehydrogenase: Biochemical and kinetic characterization. Protein Expr. Purif. 137, 20–25. https://doi.org/10.1016/j.pep.2017.06.010.

Ganjave, S.D., O'Niel, R.A., Wangikar, P.P., 2023. Rate of dilution and redox ratio influence the refolding efficiency of recombinant fungal dehydrogenases. Int. J. Biol. Macromol. 250, 126163 https://doi.org/10.1016/j.ijbiomac.2023.126163.

Garcia, S.O., Ulyanova, Y.V., Figueroa-Teran, R., Bhatt, K.H., Singhal, S., Atanassov, P., 2016. Wearable sensor system powered by a biofuel cell for detection of lactate levels in sweat. ECS J. Solid State Sci. Technol.: JSS 5, M3075–M3081. https://doi.org/10.1149/2.0131608jss.

Humer, D., Ebner, J., Spadiut, O., 2020. Scalable high-performance production of recombinant horseradish peroxidase from E. coli inclusion bodies. Int. J. Mol. Sci. 21, 4625. https://doi.org/10.3390/ijms21134625.

Humer, D., Spadiut, O., 2018. Wanted: more monitoring and control during inclusion body processing. World J. Microbiol. Biotechnol. 34, 158. https://doi.org/10.1007/s11274-018-2541-5.

Istrate, O., Rotariu, L., Bala, C., 2021. Amperometric L-lactate biosensor based upon a gold nanoparticles/reduced graphene oxide/polyallylamine hydrochloride modified screen-printed graphite electrode. Chemosensors 9, 74. https://doi.org/10.3390/chemosensors9040074.

Jia, J., Mu, W., Zhang, T., Jiang, B., 2010. Bioconversion of phenylpyruvate to phenyllactate: gene cloning, expression, and enzymatic characterization of d- and l1-lactate dehydrogenases from lactobacillus plantarum SK002. Appl. Biochem. Biotechnol. 162, 242–251. https://doi.org/10.1007/s12010-009-8767-9.

Jiang, T., Xu, Y., Sun, X., Zheng, Z., Ouyang, J., 2014. Kinetic characterization of recombinant Bacillus coagulans FDP-activated l-lactate dehydrogenase expressed in Escherichia coli and its substrate specificity. Protein Expr. Purif. 95, 219–225. https://doi.org/10.1016/j.pep.2013.12.014.

Kopp, J., Slouka, C., Spadiut, O., Herwig, C., 2019. The rocky road from fed-batch to continuous processing With E. coli. Front. Bioeng. Biotechnol. 7, 328. https://doi.org/10.3389/fbioe.2019.00328.

Kopp, J., Slouka, C., Ulonska, S., Kager, J., Fricke, J., Spadiut, O., Herwig, C., 2018. Impact of glycerol as carbon source onto specific sugar and inducer uptake rates and inclusion body productivity in E. coli BL21(DE3). Bioengineering 5, 1. https://doi.org/10.3390/bioengineering5010001 number: 1 Publisher: Multidisciplinary Digital Publishing Institute.

Kopp, J., Zauner, F.B., Pell, A., Hausjell, J., Humer, D., Ebner, J., Herwig, C., Spadiut, O., Slouka, C., Pell, R., 2020. Development of a generic reversed-phase liquid chromatography method for protein quantification using analytical quality-by-

design principles. J. Pharm. Biomed. Anal. 188, 113412 https://doi.org/10.1016/j.jpba.2020.113412.
Kucherenko, I.S., Topolnikova, Y.V., Soldatkin, O.O., 2019. Advances in the biosensors for lactate and pyruvate detection for medical applications: A review. TrAC Trends Anal. Chem. 110, 160–172. https://doi.org/10.1016/j.trac.2018.11.004.
Kumar, N., Lin, Y.J., Huang, Y.C., Liao, Y.T., Lin, S.P., 2023. Detection of lactate in human sweat via surface-modified, screen-printed carbon electrodes. Talanta 265, 124888. https://doi.org/10.1016/j.talanta.2023.124888.
Laemmli, U.K., 1970. Cleavage of structural proteins during the assembly of the head of bacteriophage T4. Nature 227, 680–685. https://doi.org/10.1038/227680a0.
Leyva-Carrillo, L., Hernandez-Palomares, M., Valenzuela-Soto, E.M., Figueroa-Soto, C.G., Yepiz-Plascencia, G., 2019. Purification and partial biochemical characterization of recombinant lactate dehydrogenase 1 (LDH-1) of the white shrimp Litopenaeus vannamei. Protein Expr. Purif. 164, 105461 https://doi.org/10.1016/j.pep.2019.105461.
Luo, X., Zhang, Y., Yin, F., Hu, G., Jia, Q., Yao, C., Fu, Y., 2020. Enzymological characterization of a novel d-lactate dehydrogenase from Lactobacillus rossiae and its application in d-phenyllactic acid synthesis. 3 Biotech 10, 101. https://doi.org/10.1007/s13205-020-2098-5.
Margreiter, G., Schwanninger, M., Bayer, K., Obinger, C., 2008. Impact of different cultivation and induction regimes on the structure of cytosolic inclusion bodies of TEM1-β-lactamase. Biotechnol. J. 3, 1245–1255. https://doi.org/10.1002/biot.200800072.
Nadeem, M.S., Al-Ghamdi, M.A., Khan, J.A., Sadath, S., Al-Malki, A., 2018. Recombinant production and biochemical and in silico characterization of lactate dehydrogenase from Geobacillus thermodenitrificans DSM-465. Electron. J. Biotechnol. 35, 18–24. https://doi.org/10.1016/j.ejbt.2018.06.003.
Nadeem, M.S., Moran, J., Murtaza, B.N., Muhammad, K., Ahmad, H., 2014. Cloning, E. coli expression, and characterization of heart lactate dehydrogenase B from river buffalo (Bubalus bubalis). Anim. Biotechnol. 25, 23–34. https://doi.org/10.1080/10495398.2013.804832 (publisher: Taylor & Francis).
Nowicki, M.W., Blackburn, E.A., McNae, I.W., Wear, M.A., 2015. A Streamlined, Automated protocol for the production of milligram quantities of untagged recombinant rat lactate dehydrogenase a using ÄKTAxpressTM. PLOS ONE 10, e0146164. https://doi.org/10.1371/journal.pone.0146164 (publisher: Public Library of Science).
Nural, B., Erdemir, A., Mutlu, O., Yakarsonmez, S., Danis, O., Topuzogullari, M., Turgut-Balik, D., 2016. Biochemical and in silico Characterization of Recombinant L-Lactate Dehydrogenase of Theileria annulata. Mol. Biotechnol. 58, 256–267. https://doi.org/10.1007/s12033-016-9924-3.
Pauk, J.N., RajuPalanisamy, J., Kager, J., Koczka, K., Berghammer, G., Herwig, C., Veiter, L., 2021. Advances in monitoring and control of refolding kinetics combining PAT and modeling. Appl. Microbiol. Biotechnol. 105, 2243–2260. https://doi.org/10.1007/s00253-021-11151-y.
Pekarsky, A., Konopek, V., Spadiut, O., 2019. The impact of technical failures during cultivation of an inclusion body process. Bioprocess Biosyst. Eng. 42, 1611–1624. https://doi.org/10.1007/s00449-019-02158-x.
Puranik, N., Parihar, A., Raikwar, J., Khandia, R., 2021. Lactate dehydrogenase a potential diagnostic biomarker for cancer: a review of literature. biomedical. J. Sci. Tech. Res. 38, 30426–30432. https://doi.org/10.26717/BJSTR.2021.38.006164 (company: Biomedres Distributor: Biomedres Institution: Biomedres Label: Biomedres Publisher: Biomedical Research Network+, LLC).
Rathee, K., Dhull, V., Dhull, R., Singh, S., 2016. Biosensors based on electrochemical lactate detection: A comprehensive review. Biochem. Biophys. Rep. 5, 35–54. https://doi.org/10.1016/j.bbrep.2015.11.010.
Rayappan, J.B.B., Nesakumar, N., Bhat, L.R., Gumpu, M.B., Babu, K.J., Jayalatha JBB, A., 2019. Electrochemical Biosensors with Nanointerface for Food, Water Quality, and Healthcare Applications. Bioelectrochemical Interface Engineering. John Wiley & Sons, Ltd,, pp. 431–468. https://doi.org/10.1002/9781119611103.ch22 section: 22.
Satomura, T., Hayashi, J., Sakamoto, H., Nunoura, T., Takaki, Y., Takai, K., Takami, H., Ohshima, T., Sakuraba, H., Suye, S.I., 2018. d-Lactate electrochemical biosensor prepared by immobilization of thermostable dye-linked d-lactate dehydrogenase from Candidatus Caldiarchaeum subterraneum. J. Biosci. Bioeng. 126, 425–430. https://doi.org/10.1016/j.jbiosc.2018.04.002.
Siew, Y.Y., Zhang, W., 2021. Downstream processing of recombinant human insulin and its analogues production from E. coli inclusion bodies. Bioresour. Bioprocess. 8, 65. https://doi.org/10.1186/s40643-021-00419-w.
Singh, A., Upadhyay, V., Upadhyay, A.K., Singh, S.M., Panda, A.K., 2015. Protein recovery from inclusion bodies of Escherichia coli using mild solubilization process. Microb. Cell Factor. 14, 41. https://doi.org/10.1186/s12934-015-0222-8.
Singh, V., Kaushal, D.C., Rathaur, S., Kumar, N., Kaushal, N.A., 2012. Cloning, overexpression, purification and characterization of Plasmodium knowlesi lactate dehydrogenase. Protein Expr. Purif. 84, 195–203. https://doi.org/10.1016/j.pep.2012.05.008.
Singhvi, P., Saneja, A., Srichandan, S., Panda, A.K., 2020. Bacterial inclusion bodies: a treasure trove of bioactive proteins. Trends Biotechnol. 38, 474–486. https://doi.org/10.1016/j.tibtech.2019.12.011.
Slouka, C., Kopp, J., Hutwimmer, S., Strahammer, M., Strohmer, D., Eitenberger, E., Schwaighofer, A., Herwig, C., 2018. Custom made inclusion bodies: impact of classical process parameters and physiological parameters on inclusion body quality attributes. Microb. Cell Factor. 17, 148. https://doi.org/10.1186/s12934-018-0997-5.
Slouka, C., Kopp, J., Spadiut, O., Herwig, C., 2019. Perspectives of inclusion bodies for bio-based products: curse or blessing? Appl. Microbiol. Biotechnol. 103, 1143–1153. https://doi.org/10.1007/s00253-018-9569-1.
Sun, Y., Gao, G., Cai, T., 2021. Enzymatic characterization of D-lactate dehydrogenase and application in alanine aminotransferase activity assay kit. Bioengineered 12, 6459–6471. https://doi.org/10.1080/21655979.2021.1972781.
Togashi, H., Nara, T., Sekikawa, C., Kawakami, M., Yaginuma, N., Tsunoda, T., Sakaguchi, K., Mizukami, F., 2009. Refolding of lactate dehydrogenase by zeolite beta. Biotechnol. Prog. 25, 200–206. https://doi.org/10.1002/btpr.107.
Torkzadeh-Mahani, M., Zaboli, M., Barani, M., Torkzadeh-Mahani, M., 2020. A combined theoretical and experimental study to improve the thermal stability of recombinant D-lactate dehydrogenase immobilized on a novel superparamagnetic Fe3O4NPs@metal-organic framework. Appl. Organomet. Chem. 34, e5581 https://doi.org/10.1002/aoc.5581.
Tsai, Y.C., Chen, S.Y., Liaw, H.W., 2007. Immobilization of lactate dehydrogenase within multiwalled carbon nanotube-chitosan nanocomposite for application to lactate biosensors. Sens. Actuators B: Chem. 125, 474–481. https://doi.org/10.1016/j.snb.2007.02.052.
Vanderlinde, R.E., 1985. Measurement of Total Lactate Dehydrogenase Activity. Ann. Clin. Lab. Sci.
Yamaguchi, H., Miyazaki, M., 2014. Refolding techniques for recovering biologically active recombinant proteins from inclusion bodies. Biomolecules 4, 235–251. https://doi.org/10.3390/biom4010235.
Zaboli, M., Saeidnia, F., Zaboli, M., Torkzadeh-Mahani, M., 2021. Stabilization of recombinant d-Lactate dehydrogenase enzyme with trehalose: response surface methodology and molecular dynamics simulation study. Process Biochem. 101, 26–35. https://doi.org/10.1016/j.procbio.2020.11.001.
Zhou, X., Zhou, J., Xin, F., Ma, J., Zhang, W., Wu, H., Jiang, M., Dong, W., 2018. Heterologous expression of a novel d-lactate dehydrogenase from Lactobacillus sp. ZX1 and its application for d-phenyllactic acid production. Int. J. Biol. Macromol. 119, 1171–1178. https://doi.org/10.1016/j.ijbiomac.2018.08.036.
Zhu, S., Gong, C., Ren, L., Li, X., Song, D., Zheng, G., 2013. A simple and effective strategy for solving the problem of inclusion bodies in recombinant protein technology: His-tag deletions enhance soluble expression. Appl. Microbiol. Biotechnol. 97, 837–845. https://doi.org/10.1007/s00253-012-4630-y.